PCCP

PAPER

View Article Online
View Journal | View Issue

Cite this: *Phys. Chem. Chem. Phys.*, 2017, **19**, 31655

$B_{12}F_n^{0/-}$ (n = 1–6) series: when do boron double chain nanoribbons become global minima?†

Hui Bai, ‡[a] Bing Bai,‡[a] Lin Zhang,[a] Wei Huang, *[a] Hua-Jin Zhai *[b] and Si-Dian Li *[b]

We present an extensive density-functional and wave function theory study of partially fluorinated $B_{12}F_n^{0/-}$ (n = 1–6) series, which show that the global minima of $B_{12}F_n^{0/-}$ (n = 2–6) are characterized to encompass a central boron double chain (BDC) nanoribbon and form stable BF_2 groups at the corresponding BDC corner when $n \geq 3$, but the $B_{12}F^{0/-}$ system maintains the structural feature of the well-known quasi-planar C_{3v} B_{12}. When we put the spotlight on $B_{12}F_6^{0/-}$ species, our single-point CCSD(T) results unveil that albeit with the 3D icosahedral isomers not being their global minima, C_2 $B_{12}F_6$ (**6.1**, ^{1}A) and C_1 $B_{12}F_6^-$ (**12.1**, ^{2}A) as typical low-lying isomers are 0.60 and 1.95 eV more stable than their 2D planar counterparts D_{3h} $B_{12}F_6$ (**6.7**, ^{1}A′) and C_{2v} $B_{12}F_6^-$ (**12.7**, $^2A_2$), respectively, alike to $B_{12}H_6^{0/-}$ species in our previous work. Detailed bonding analyses suggest that $B_{12}F_n^{0/-}$ (n = 2–5) possess ribbon aromaticity with σ plus π double conjugation along the BDC nanoribbon on account of their total number of σ and π delocalized electrons conforming the common electron configuration ($\pi^{2(n+1)}\sigma^{2n}$). Furthermore, the simulated PES spectra of the global minima of $B_{12}F_n^-$ (n = 1–6) monoanions may facilitate their experimental characterization in the foreseeable future. Our work provides new examples for ribbon aromaticity and powerful support for the F/H/Au/BO analogy.

Received 18th August 2017,
Accepted 7th November 2017

DOI: 10.1039/c7cp05658c

rsc.li/pccp

1. Introduction

As the prototype of electron deficient elements characterized with multicenter bonds in planar networks or cage-like structures, boron clusters have attracted almost unprecedented attention over the past decade in the area of cluster science. The joint photoelectron spectroscopy (PES) and high-level theoretical calculations have indicated that the global minima for B_n^- exhibit planar or quasi-planar structures up to n = 38,[1,2] as well as B_{40}^-,[3] that are unparalleled in any other elements in the periodic table. Furthermore, cationic B_n^+ and neutral B_n clusters also were revealed to favor 2D structures at least up to n = 16[4] and n = 20,[5] respectively.

Among all boron clusters characterized so far, neutral B_{12} shows unique electronic and structural properties.[6] Quasi-planar C_{3v} B_{12} is an aromatic system with six π electrons and possesses a 2.0 eV first excitation energy which is the greatest of all B_n (n = 3–23) clusters. Therefore, compound clusters based on B_{12} have been actively pursued,[7–12] in particular partial hydrogenation that is expected to address the 2D-to-3D structural evolution by breaking the peripheral B–B σ bonds. As the icosahedral $B_{12}H_{12}^{2-}$ is known to be the most stable polyhedral borane,[7,13] it initially motivates people to address the planar to cage structural transformation in $B_{12}H_n$ as a function of hydrogen content. This 2D-to-3D structural transition for $B_{12}H_n^+$ (n = 0–12) clusters has been suggested to occur at $B_{12}H_6^+$.[12] Subsequently, a planar D_{3h} borozene molecule $B_{12}H_6$ was proposed[7] and its potential of being a building block for large aromatic compounds also was explored.[7,8,14] However, our systematic theoretical investigation of $B_{12}H_n$ (n = 1–8) showed that the proposed borozene $B_{12}H_6$ structure is just a high-lying local minimum[10] and the computational results also revealed that there exists a planar-to-cage structural transition for $B_{12}H_n^{+/0/-}$ species at around n = 4.[7,9,10] It is well-known that the 2D-to-3D structural transformation can be influenced by means of adding hydrogen, fluorine or heavier halides.[15,16] Hence, a density functional theory and quantum Monte Carlo calculation claimed that the 2D $B_{12}F_n$ (n = 0–4) clusters, which are based on the structure of C_{3v} B_{12},[6] are more stable than the corresponding

[a] *Key Laboratory of Coal Science and Technology of Ministry of Education and Shanxi Province, Taiyuan University of Technology, Taiyuan 030024, Shanxi, China. E-mail: huangwei@tyut.edu.cn*

[b] *Nanocluster Laboratory, Institute of Molecular Science, Shanxi University, Taiyuan 030006, Shanxi, China. E-mail: hj.zhai@sxu.edu.cn, lisidian@sxu.edu.cn*

† Electronic supplementary information (ESI) available: Low-lying isomers of $B_{12}F_n$ (n = 1–6), with their relative energies indicated in eV at CCSD(T)//B3LYP and B3LYP/6-311++G(d,p) (*in italic*) levels; low-lying isomers of $B_{12}F_n^-$ (n = 1–6), with their relative energies indicated in eV at CCSD(T)//B3LYP and B3LYP/6-311++G(d,p) (*in italic*) levels; simulated photoelectron spectra based on the global minimum C_s $B_{12}F^-$ (**7**, ^{1}A′) (a) and its low-lying isomer C_1 $B_{12}F^-$ (**7.1**, ^{1}A) (b). The simulations were done by fitting the distribution of the calculated VDEs with unit-area Gaussian functions of 0.1 eV halfwidth. See DOI: 10.1039/c7cp05658c

‡ These authors contributed equally to this work.

3D icosahedral structures and the fluorinated borozene D_{3h} $B_{12}F_6$ is energetically more favorable than its 3D counterpart at the B3LYP level.[7]

However, according to our previous calculation experiences,[10,17] B3LYP often overestimates the stability of 2D structures and the energetics from B3LYP deviate substantially from CCSD(T) for boron-based clusters. Moreover, to the best of our knowledge, few reports on the $B_{12}F_n$ ($n < 12$) system have been published up to now, except for some study on polyboron fluorides B_nF_m ($n \leq m$)[15,18] and fluoro-borane $B_{12}H_{12-n}F_n^{2-}$.[19,20] Initially, the nucleophilic substitution of hydrogen atoms in $B_{12}H_{12}^{2-}$ by F up to $B_{12}F_{12}^{2-}$ was studied.[19] According to the structures of $B_{12}H_{12-n}F_n^{2-}$ (n = 2, 4, 5, 6, 7, 8, 10, 12) and the results of quantum chemistry calculations of the charge distribution on relevant various isomers, *closo*-$B_{12}H_{12}^{2-}$ behaves in these substitution reactions as a spatial aromatic system. Furthermore, the fully fluorinated boron hydride $B_{12}F_{12}^{2-}$ was synthesized firstly, which is similar to $B_{12}H_{12}^{2-}$ and also possesses an icosahedral structure.[19] Then the preparation and spectroscopic characterization of $B_{12}H_{11}F^{2-}$ were reported.[21] Owing to the reactivity of metal ions in $M^{n+}(B_{12}F_{12})_m$ salts similar to the corresponding gas-phase M^{n+} cation, $B_{12}F_{12}^{2-}$, that is called a superweak anion, creates new opportunities for delivery of highly reactive catalysts.[22,23] Based on the above discussion, it is thus essential and of interest to systematically investigate partiality fluorinated boron hydride $B_{12}F_n$ ($n < 12$) species from the fundamental point of view for their application in the future.

Here we undertake an extensive density-functional theory (DFT) and coupled-cluster with single, double, and perturbative triple excitation [CCSD(T)] study on the partiality fluorinated boron hydride $B_{12}F_n^{0/-}$ (n = 1–6). Apart from the $B_{12}F^{0/-}$ clusters maintaining the structural feature of quasi-planar C_{3v} B_{12},[6] all $B_{12}F_n^{0/-}$ (n = 2–6) species are confirmed to possess boron double chain (BDC) nanoribbon configurations. With more F atoms being attached to $B_{12}^{0/-}$, the true global minima of $B_{12}F_n^{0/-}$ (n = 2–6) are characterized to consist of the central BDC unit with BF_2 groups, rather than the alleged quasi-planar based on C_{3v} B_{12} or icosahedral configurations. Moreover, the 2D quasi-planar D_{3h} $B_{12}F_6$ (**6.7**, ^{1}A′) is 0.60 eV less stable than the corresponding 3D icosahedral C_2 $B_{12}F_6$ (**6.1**, ^{1}A) at the CCSD(T)//B3LYP level. For the sake of exploring the properties of these BDCs with BF_2 groups, we analyzed their canonical molecular orbital (CMO) and adaptive natural density partitioning (AdNDP)[24] and revealed that all of C_{2h} $B_{12}F_2$ (**2**, ^{1}A$_g$), C_s $B_{12}F_3^-$ (**9**, ^{1}A′), C_1 $B_{12}F_4$ (**4**, ^{1}A) and C_s $B_{12}F_5^-$ (**11**, ^{1}A′) are ribbon aromatic systems in nature with $2(n+1)\pi$ plus $2n\sigma$ delocalized electrons, whose total counting overall conform to the $(4n+2)$ Hückel rule. Meanwhile, the simulated photoelectron spectra (PES) of the global minima of $B_{12}F_n^-$ (n = 1–6) may not only facilitate future experimental characterization, but also provide strong support for the F/H/Au/BO analogy.

2. Theoretical methods

Initial structures of $B_{12}F_n^{0/-}$ (n = 1–6) clusters were constructed based on quasi-planar B_{12},[6] icosahedral $B_{12}H_{12}^{2-}$[7–13] and the corresponding $B_{12}H_n^+$ cations (n = 0–12).[12] More extensive and unbiased global minimum searches were performed utilizing the Basin-Hopping procedure.[25] We optimized and analyzed the vibrational frequencies of $B_{12}F_n^{0/-}$ (n = 1–6) series using the hybrid DFT method of B3LYP[26,27] with the 6-311++G(d,p)[28] basis set as implemented in the Gaussian 09 program.[29] An additional single-point coupled cluster method including triple excitation (CCSD(T))[30] calculations with the 6-311++G(d,p) basis set was used at the B3LYP/6-311++G(d,p) geometries to further evaluate the relative energies. Our calculations proved that B3LYP indeed overestimates the stability of 2D quasi-planar isomers of $B_{12}F_n^{0/-}$ (n = 1–6) and its energetics are substantially inconsistent with CCSD(T). As a comparison, we also optimized some representative isomers of $B_{12}F_n^{0/-}$ (n = 1–6) clusters at the PBE1PBE level.[30] The AdNDP analyses were performed to elucidate the bonding patterns using the Multiwfn program.[31] AdNDP bonding patterns in Fig. 5 were visualized using the Molekel 5.4 software.[32] Excitation energies of the neutral $B_{12}F_n$ (n = 1–6) species were calculated with the time-dependent DFT (TD-DFT) method[33] at the ground-state structures of the corresponding $B_{12}F_n^-$ (n = 1–6) monoanions. The adiabatic detachment energies (ADEs) of the anions were calculated as the energy differences between the anions and the corresponding neutrals at their ground-state structures, whereas the vertical detachment energies (VDEs) were calculated as the energy differences between the ground states of the anions and the ground states of neutrals at the anionic geometries.

3. Results and discussion

3.1 The global minima and low-lying isomers of $B_{12}F_n^{0/-}$ (n = 1–6)

Combining B3LYP and CCSD(T) calculations, we obtain the global minima of $B_{12}F_n^{0/-}$ (n = 1–6) and summarize their structures, symmetries, electronic states and relative energies in eV at CCSD(T)//B3LYP and B3LYP in Fig. 1. Both their typical 2D quasi-planar isomers based on C_{3v} B_{12} and 3D icosahedral isomers are also depicted in Fig. 1. The top 8 low-lying isomers of $B_{12}F_n$ (n = 1–6) and $B_{12}F_n^-$ (n = 1–6) clusters are summarized in Fig. S1–S6 and S7–S12 in the ESI,† respectively. The energy differences of $B_{12}F_n^{0/-}$ (n = 1–6) between global minima and 2D quasi-planar isomers and between global minima and 3D icosahedral isomers are shown in Fig. 2. And the CCSD(T)//B3LYP results are mainly discussed, unless stated otherwise.

As shown in Fig. 1, we start from the global minima of $B_{12}F^{0/-}$, C_1 $B_{12}F$ (**1**, ^{2}A) and C_s $B_{12}F^-$ (**7**, ^{1}A′), which are almost the isoenergetic isomers of C_1 $B_{12}F$ (**1.1**, ^{2}A) and C_1 $B_{12}F^-$ (**7.1**, ^{1}A) with the energy differences of less than 0.09 eV, respectively, all of them are derived from the global minima of the B_{12} cluster with the F atom bonded to its periphery, similar to $B_{12}X^{0/-}$ (X = H/Au/BO).[34] Among alternative low-lying structures identified for $B_{12}F^{0/-}$ in Fig. S1 and S7 (ESI†), the BDC isomers C_s $B_{12}F$ (**1.5**, ^{2}A′) and C_s $B_{12}F^-$ (**7.5**, ^{1}A′) are 0.58 and 0.75 eV higher in energy, respectively. The well-known 3D icosahedral isomers C_1 $B_{12}F$ (**1.7**, ^{2}A) and C_s $B_{12}F^-$ (**7.7**, ^{1}A′) lie even higher above their global minima

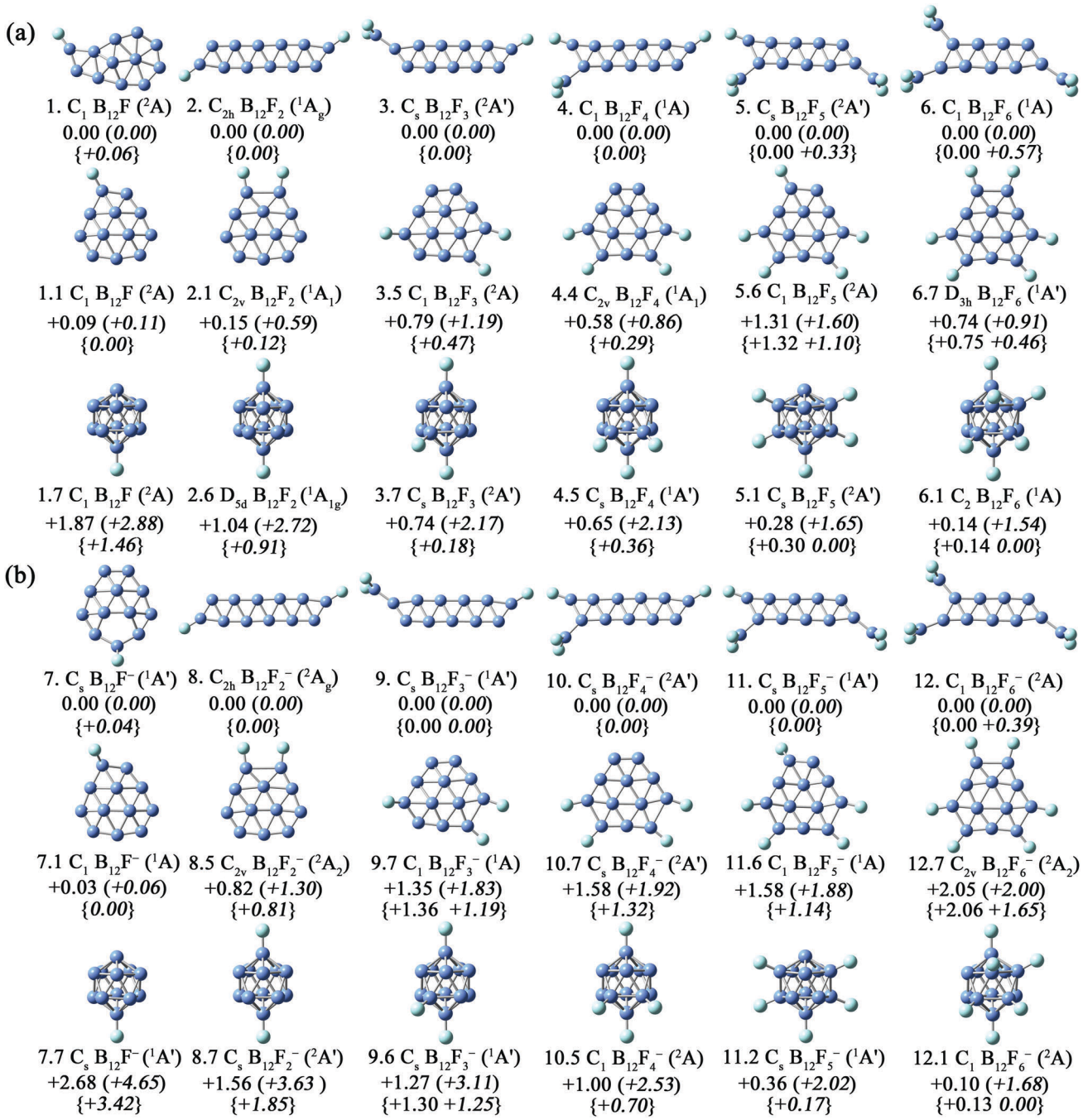

Fig. 1 Optimized global-minimum structures, typical 2D quasi-planar and 3D icosahedral isomers at the B3LYP level for (a) $B_{12}F_n$ and (b) $B_{12}F_n^-$ (n = 0–6). The symmetry, electronic state and relative energy in eV at CCSD(T)//B3LYP, B3LYP/6-311++G(d,p) (*italic*), PBE1PBE/6-311++G(d,p) (*italic* in curly brackets) and CCSD(T)//PBE1PBE (in curly brackets, for some isomers) are labeled under each structure. Boron is in blue, and F is in light green.

by 1.87 and 2.68 eV, respectively. It is clear in Fig. 1 that the global minima C_{2h} $B_{12}F_2$ (**2**, ^1A_g) and C_{2h} $B_{12}F_2^-$ (**8**, ^2A_g) all possess BDC nanoribbon structures, closely resembling the global minima of $B_{12}H_2^{0/-}$ and $B_{12}(BO)_2^{0/-}$.[35–37] C_{2v} $B_{12}F_2$ (**2.1**, $^1A_1$) and C_{2v} $B_{12}F_2^-$ (**8.5**, $^2A_2$), the quasi-planar isomers based on the configuration of C_{3v} B_{12}, are 0.15 and 0.82 eV higher in energy than their true minima, respectively. The corresponding icosahedral D_{5d} $B_{12}F_2$ (**2.6**, $^1A_{1g}$) and C_s $B_{12}F_2^-$ (**8.7**, ^{2}A′) are much less stable with a relative energy of 1.04 and 1.56 eV, respectively. The C_s $B_{12}F_2$ (**2.7** ^{1}A′) and C_s $B_{12}F_2^-$ (**8.6**, ^{2}A′) isomers with a central BDC B_{11} unit and one BF_2 group bonded to its periphery lie 1.51 and 0.91 eV higher in energy than their corresponding global minima, separately. Other isomers of $B_{12}F_2^{0/-}$ are also displayed in Fig. S2 and S8 (ESI†). When another F atom is introduced to $B_{12}F_2^{0/-}$, C_s $B_{12}F_3$ (**3**, ^{2}A′) and C_s $B_{12}F_3^-$ (**9**, ^{1}A′), accompanied by the structural feature of BDC with one F atom and one BF_2 group bonding to the central B_{11} unit, turn out to be their global minima, respectively.

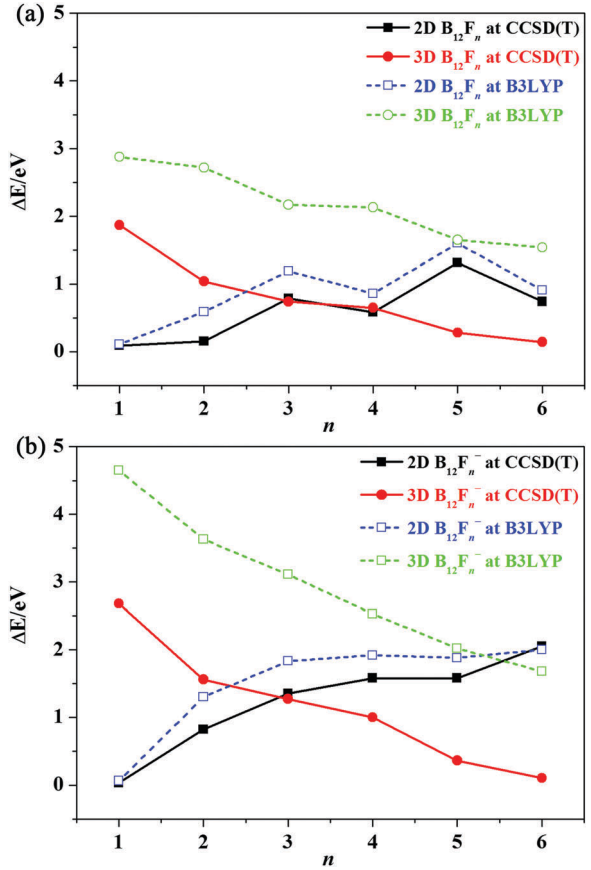

Fig. 2 The energy difference curves of $B_{12}F_n$ (n = 1–6) (a) and $B_{12}F_n^-$ (n = 1–6) (b) between global-minimum structures and quasi-planar (2D) isomers (black solid squares at CCSD(T) and blue empty squares at B3LYP), global-minimum structures and icosahedral (3D) isomers (red solid dots at CCSD(T) and green empty dots at B3LYP) at CCSD(T) and B3LYP levels.

However, as shown in Fig. S3 and S9 (ESI†), the BDC planar nanoribbons without BF_2 group C_s $B_{12}F_3$ (**3.1**, $^2A'$) and C_s $B_{12}F_3^-$ (**9.1**, $^1A'$) are proved to be the second candidates with the relative energy values of 0.31 and 0.74 eV. Among higher isomers are 2D quasi-planar C_1 $B_{12}F_3$ (**3.5**, ^2A) and C_1 $B_{12}F_3^-$ (**9.7**, ^1A), situating at 0.79 and 1.35 eV above C_s $B_{12}F_3$ (**3**, $^2A'$) and C_s $B_{12}F_3^-$ (**9**, $^1A'$), respectively. Similarly, the typical icosahedral isomers C_s $B_{12}F_3$ (**3.7**, $^2A'$) and C_s $B_{12}F_3^-$ (**9.6**, $^1A'$) are all at least 0.74 eV above their global minima. It is a remarkable fact that 3D icosahedral C_s $B_{12}F_3$ (**3.7**, $^2A'$) and C_s $B_{12}F_3^-$ (**9.6**, $^1A'$) have been found to be more stable than 2D quasi-planar C_1 $B_{12}F_3$ (**3.5**, ^2A) and C_1 $B_{12}F_3^-$ (**9.7**, ^1A) at the CCSD(T) level, respectively. In fact, C_1 $B_{12}F_3$ (**3.5**, ^2A) and C_s $B_{12}F_3$ (**3.7**, $^2A'$) can be viewed as isoenergetic isomers.

With more F atoms being attached to $B_{12}^{0/-}$, the global minima of $B_{12}F_4^{0/-}$ are similar to that of $B_{12}F_3^{0/-}$. Our sufficient calculations show that C_1 $B_{12}F_4$ (**4**, ^1A) and C_s $B_{12}F_4^-$ (**10**, $^2A'$) are the most stable structures with the BDC B_{11} unit which is bonded with two F atoms directly and one BF_2 group by one B–B bond at its periphery. Compared with other low-lying isomers with a BDC motif for the $B_{12}F_4$ cluster in Fig. S4 (ESI†), both C_{2h} $B_{12}F_4$ (**4.6**, ^1A_g) consisting of the BDC B_{10} unit with two BF_2 groups and C_{2h} $B_{12}F_4$ (**4.7**, ^1A_g) composing of the BDC B_{12} unit with four B–F bonds are at least 0.67 eV above the global-minimum C_1 $B_{12}F_4$ (**4**, ^1A). The popular 2D quasi-planar isomer C_{2v} $B_{12}F_4$ (**4.4**, $^1A_1$) and 3D icosahedral isomer C_s $B_{12}F_4$ (**4.5**, $^1A'$) are 0.58 and 0.65 eV higher in energy, respectively. For $B_{12}F_4^-$, the C_{2h} $B_{12}F_4^-$ (**10.1**, ^2A_g) BDC isomer with two BF_2 groups is found to be nearly degenerate with the global-minimum C_s $B_{12}F_4^-$ (**10**, $^2A'$) and the energy difference is merely 0.09 eV. C_2 $B_{12}F_4^-$ (**10.6**, ^2A), as the other available BDC isomer, lies 1.53 eV higher in energy. As indicated in Fig. 1, the 3D icosahedral C_1 $B_{12}F_4^-$ (**10.5**, ^2A) becomes more stable than the 2D quasi-planar C_s $B_{12}F_4^-$ (**10.7**, $^2A'$) in spite of both of them being at least 1.00 eV less stable than the global-minimum C_s $B_{12}F_4^-$ (**10**, $^2A'$). With one more F atom being attached to $B_{12}F_4^{0/-}$, the global minimum searches in conjunction with full structural optimizations found that C_s $B_{12}F_5$ (**5**, $^2A'$) and C_s $B_{12}F_5^-$ (**11**, $^1A'$) are the global minima of $B_{12}F_5^{0/-}$ species, which are derived from the BDC B_{10} unit with two BF_2 groups and one F atom bonding to its periphery. The fact is that the global minima of $B_{12}F_5^{0/-}$ closely resemble the counterparts of $B_{12}F_4^{0/-}$. As shown in Fig. 1 and Fig. S5, S12 (ESI†), both the 3D icosahedral C_s $B_{12}F_5$ (**5.1**, $^2A'$) and C_s $B_{12}F_5^-$ (**11.2**, $^1A'$) nearly become the nearest low-lying isomers and lie 0.28 and 0.36 eV higher in energy, respectively. However, the 2D quasi-planar C_1 $B_{12}F_5$ (**5.6**, ^2A) and C_1 $B_{12}F_5^-$ (**11.6**, ^1A) are proved to be 1.31 and 1.58 eV less stable than their corresponding global minima. When the total number of F atoms reaches six, we found that the true minima C_1 $B_{12}F_6$ (**6**, ^1A) and C_1 $B_{12}F_6^-$ (**12**, ^2A) stem from the global minima C_s $B_{12}F_5$ (**5**, $^2A'$) and C_s $B_{12}F_5^-$ (**11**, $^1A'$) by means of breaking a B–B bond in the central B_{10} unit and forming a new BF_2 group. Surprisingly, the well-known 3D icosahedral or called cage-like C_2 $B_{12}F_6$ (**6.1**, ^1A) and C_1 $B_{12}F_6^-$ (**12.1**, ^2A) turn out to be the nearest isomers with the relative energy values of 0.14 and 0.10 eV, respectively. In contrast, the popular 2D quasi-planar D_{3h} $B_{12}F_6$ (**6.7**, $^1A'$) and C_{2v} $B_{12}F_6^-$ (**12.7**, $^2A_2$) are confirmed to be the most unstable isomers among the top 8 low-lying candidates, which are 0.74 and 2.05 eV above their corresponding global minima. As shown in Fig. 1, we also found that the relative energy orders of $B_{12}F_n$ (n = 1–4) and $B_{12}F_n^-$ (n = 1–5) species at the PBE1PBE level are almost consistent with that at CCSD(T)//B3LYP. Moreover, except for $B_{12}H_2^-$ (**8.7**) (its symmetry is C_s at B3LYP but C_1 at PBE1PBE.), the geometries of $B_{12}F_n^{0/-}$ (n = 1–6) species at PBE1PBE well agree with their counterparts at B3LYP. However, the PBE1PBE results show that the 2D quasi-planar C_1 $B_{12}F_3^-$ (**9.7**, ^1A) is slightly more stable than the 3D icosahedral C_s $B_{12}F_3^-$ (**9.6**, $^1A'$). The 3D icosahedral C_s $B_{12}F_5$ (**5.1**, $^2A'$) is more stable than the BDC nanoribbon C_s $B_{12}F_5$ (**5**, $^2A'$) and 2D quasi-planar C_1 $B_{12}F_5$ (**5.6**, ^2A) at the PBE1PBE level, with the relative energy values of 0.33 and 1.10 eV, respectively. Similarly, the 3D icosahedral $B_{12}F_6^{0/-}$ species are proved to be the most stable isomers with respect to their BDC nanoribbon and 2D quasi-planar isomers. After the single point calculations for $B_{12}F_3^-$, $B_{12}F_5$ and $B_{12}F_6^{0/-}$ species based on their optimized structures at PBE1PBE, we verified that the relative energies from CCSD(T)// PBE1PBE are in good agreement with the CCSD(T)//B3LYP results,

as displayed in Fig. 1. Therefore, there is no large effect on their relative energies obtained using the B3LYP or PBE1PBE method as long as the single-point CCSD(T) calculations are performed at the corresponding geometries eventually. In addition, the 3D icosahedral C_2 $B_{12}F_6$ (**6.1**, ^{1}A) is more stable than BDC nanoribbon C_1 $B_{12}F_6$ (**6**, ^{1}A) and 2D quasi-planar D_{3h} $B_{12}F_6$ (**6.7**, ^{1}A′) at the MP2/6-311++G(d,p) level, with the relative energy values of 0.90 and 1.15 eV, respectively. However, at the CCSD(T)//MP2 level, the BDC nanoribbon C_1 $B_{12}F_6$ (**6**, ^{1}A) is proved to be 0.12 and 0.74 eV more stable than 3D icosahedral C_2 $B_{12}F_6$ (**6.1**, ^{1}A) and 2D quasi-planar D_{3h} $B_{12}F_6$ (**6.7**, ^{1}A′), respectively. It can be seen that the CCSD(T)//MP2 results are also well consistent with the CCSD(T)//B3LYP results.

For a better comparison with the representative 2D quasi-planar and 3D icosahedral isomers of the $B_{12}F_n^{0/-}$ (n = 1–6) system, we plotted relative energy difference curves as a function of the number of F atoms n. As clearly shown in Fig. 2, no matter what species, either $B_{12}F_n$ or $B_{12}F_n^-$, both the variation trend of the energy difference between global minima and 2D quasi-planar isomers and the relevant trend between global minima and 3D icosahedral isomers at the CCSD(T) level are in good agreement with that at the B3LYP level, and it can be described as the relative stabilities of 3D icosahedral isomers gradually increase but the relative stabilities of 2D quasi-planar ones decrease step by step, along with the increasing of F atoms. Compared with the CCSD(T) and B3LYP results, there is no doubt that B3LYP distinctly overestimates the relative energy values of 2D and 3D isomers. For $B_{12}F_n$ (n = 1–6), the 2D quasi-planar isomers are more stable than their corresponding 3D icosahedral isomers at the B3LYP level, however, as can be seen from the figure at more accurate CCSD(T) level, when the number of F atoms equals to 3–4, 3D C_s $B_{12}F_3$ (**3.7**, ^{2}A′) and C_s $B_{12}F_4$ (**4.5**, ^{1}A′) turn out to be energetically competitive with 2D C_1 $B_{12}F_3$ (**3.5**, ^{2}A) and C_{2v} $B_{12}F_4$ (**4.4**, $^1A_1$), respectively, and when n is greater than 4, 3D isomers become more stable. For the $B_{12}F_n^-$ (n = 1–6) system, similar to the case of $B_{12}F_n$ at B3LYP, the 2D quasi-planar $B_{12}F_n^-$ (n = 1–5) are proved to be at least 0.14 eV more stable than their 3D icosahedral isomers, only the 3D icosahedral C_1 $B_{12}F_6^-$ (**12.1**, ^{2}A) turns out to be favored in energy (0.32 eV) over the 2D quasi-planar C_{2v} $B_{12}F_6^-$ (**12.7**, $^2A_2$). Nevertheless, we further calculated the relative energy of $B_{12}F_n^-$ using the more accurate CCSD(T) method at B3LYP structures and found that the 3D and 2D structures of $B_{12}F_3^-$ can be practically viewed as iso-energetic isomers. When $n > 3$, the 3D icosahedral isomers are energetically more favored than their 2D quasi-planar counterparts. Based on the above theoretical calculation results, the fact is B3LYP undisputedly overestimates the stability of the 2D quasi-planar structures of $B_{12}F_n^{0/-}$ (n = 1–6).

3.2 $B_{12}F_n^{0/-}$ (n = 1–6): quasi-planar *vs.* icosahedral isomers

The 2D quasi-planar and 3D icosahedral $B_{12}H_n^{0/-}$ (n = 1–6) clusters[10] have been investigated in our previous work, and herein we have extended the research to $B_{12}F_n^{0/-}$ (n = 1–6) by using F instead of H atoms, although they are not the true minima on their potential energy surfaces. As a matter of fact, a similar work about $B_{12}F_n$ has been reported at the B3LYP level,[7] however, it is indispensable to further verify its accuracy according to our calculation experiences for boron clusters.

As a comparison, we also plotted the total energy difference between 2D quasi-planar and 3D icosahedral $B_{12}F_n^{0/-}$ (n = 1–6) species as a function of the number of F atoms. As clearly shown in Fig. 3, the variation trend of the energy difference between 2D quasi-planar and 3D icosahedral isomers at the CCSD(T) level is in good agreement with that at B3LYP and our calculation results on the variation trend of the energy difference between 2D and 3D isomers of $B_{12}F_n$ (n = 1–6) at the B3LYP level in Fig. 3(a) are in good accord with the reported results for $B_{12}F_n$ clusters,[7] which show that the 2D quasi-planar clusters with up to six H atoms are more stable than the corresponding 3D icosahedral structures. However, our CCSD(T) results verify that the 2D quasi-planar clusters of $B_{12}F_n$ (n = 1, 2) are proved to be 1.78 and 0.89 more stable than their 3D icosahedral structures, respectively. The 2D quasi-planar and 3D icosahedral isomers of $B_{12}F_n$ (n = 3, 4) can be viewed as energetically competitive configurations with a 0.05–0.07 eV energy difference. Conversely, the 2D quasi-planar structures of $B_{12}F_n$ (n = 5, 6) are 1.03 and 0.60 eV less stable than their corresponding 3D icosahedral isomers, respectively. Therefore, a 2D-to-3D structural transition actually occurs at n = 5 in partially fluorinated $B_{12}F_n$ (n = 1–6)

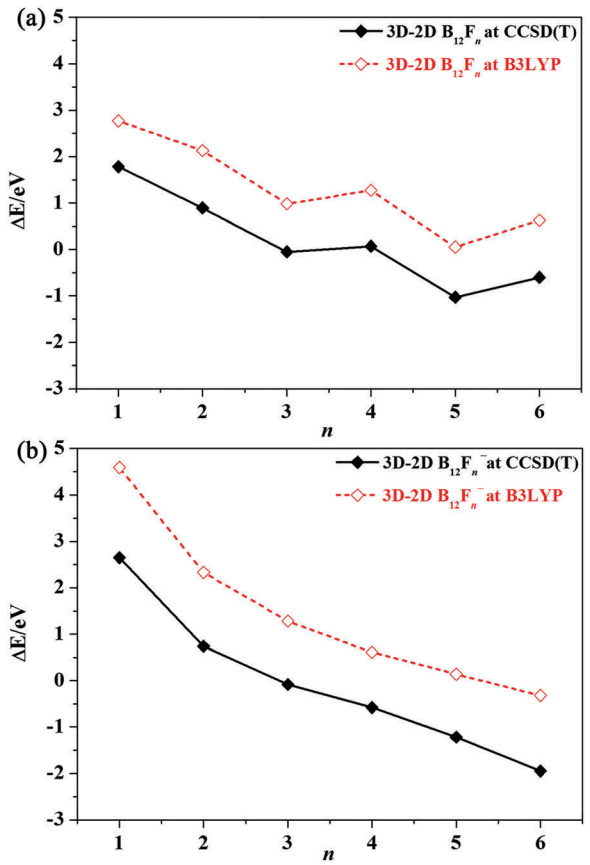

Fig. 3 The energy difference curves of $B_{12}F_n$ (n = 1–6) (a) and $B_{12}F_n^-$ (n = 1–6) (b) between quasi-planar (2D) and icosahedral (3D) isomers at CCSD(T) (black solid rhombuses) and B3LYP (red empty rhombuses) levels.

series, while a similar structural reverse occurs at n = 4 in the $B_{12}H_n$ system.[10] Considering that B3LYP overestimates the robustness of 2D quasi-planar configurations as it takes into account the electron correlation energy less sufficient than CCSD(T), hereinto we mainly discuss the CCSD(T) results for $B_{12}F_n^-$ (n = 1–6) species in Fig. 3(b). Our calculation results establish that $B_{12}F_n^-$ preferentially forms 2D quasi-planar structures in the size range between n = 1–2, whereas $B_{12}F_n^-$ (n = 3–6) tend to form 3D icosahedral cages. A stability conversion actually occurs from $B_{12}F_3^-$, with the distorted 3D icosahedral C_s $B_{12}F_3^-$ (**9.6**, $^1A'$) being 0.08 eV more stable than the corresponding 2D quasi-planar C_1 $B_{12}F_3^-$ (**9.7**, ^1A) at the CCSD(T) level. Similar to $B_{12}H_6^{0/-}$, both the 2D planar D_{3h} $B_{12}F_6$ (**6.7**, $^1A'$) and C_{2v} $B_{12}F_6^-$ (**12.7**, $^2A_2$) are just high-lying local minima of the system and can also be safely ruled out from experiments under normal conditions. Therefore, it is unfeasible to design larger boron-based nanomaterials starting from 2D planar $B_{12}F_6^{0/-}$ building blocks. Simultaneously, we found that the partial fluorination cannot reverse the relative stability of the corresponding 2D quasi-planar boron hydride counterparts.

3.3 Chemical bonding analyses

In order to shed further light on the stability of the global minima of $B_{12}F_n^{0/-}$ (n = 1–6), we analyzed their delocalized π and σ CMOs and performed chemical bonding analysis using AdNDP in the Multiwfn program[31] that represents the electronic structure of a molecule in terms of n-centre two-electron bonds (nc-2e) with n ranging from one to the total number of atoms in the molecule. Because the AdNDP method handles only closed-shell systems, we chose C_{2h} $B_{12}F_2$ (**2**, ^1A_g), C_s $B_{12}F_3^-$ (**9**, $^1A'$), C_1 $B_{12}F_4$ (**4**, ^1A), C_s $B_{12}F_5^-$ (**11**, $^1A'$), and C_1 $B_{12}F_6$ (**6**, ^1A) with 25, 29, 32, 36, and 39 electron pairs for the purpose of bonding analyses, respectively. The delocalized π and σ CMOs are presented in Fig. 4 and the detailed AdNDP results are summarized in Fig. 5.

As revealed from the CMOs in Fig. 4, the BDC nanoribbon C_{2h} $B_{12}F_2$ (**2**, ^1A_g), C_s $B_{12}F_3^-$ (**9**, $^1A'$), C_1 $B_{12}F_4$ (**4**, ^1A) and C_s $B_{12}F_5^-$ (**11**, $^1A'$) all possess three delocalized π CMOs and two delocalized σ CMOs, which conform the common electron configuration ($\pi^{2(n+1)}\sigma^{2n}$) of ribbon aromaticity[17] and the total number of delocalized electrons amounts to the $(4n + 2)$ Hückel rule. The key mechanism of ribbon aromaticity is that the optimal delocalized π and σ bondings within the B_3 or B_4 unit effectively reduce the intramolecular electrostatic repulsion in the BDC nanoribbon configuration. The ribbon aromatic system satisfies the common electron configuration of $\pi^{2(n+1)}\sigma^{2n}$, with $(n + 1)$ delocalized π CMOs and n delocalized σ CMOs. Therefore, the total number of delocalized electrons amounts to $2(n + 1)\pi + 2n\sigma$ that is the $(4n + 2)$ Hückel rule. In fact, all delocalized π and σ CMOs in the BDC nanoribbons originate from the overlaps between B 2p atomic orbitals of neighboring atoms in the single B chains. Moreover, the delocalized π and σ CMOs are highly mixed in sequence based on their energies, into which the available valence electrons in the system successively fill. When two electrons occupy a π CMO, the next two electrons would fill in a σ CMO. Because the ribbon aromaticity in the BDC structures may be conveniently achieved either by an appropriate number of B atoms, or by charging, or both of them, C_1 $B_{12}F_6$ (**6**, ^1A) with a B_9 BCD unit does not belong to the ribbon

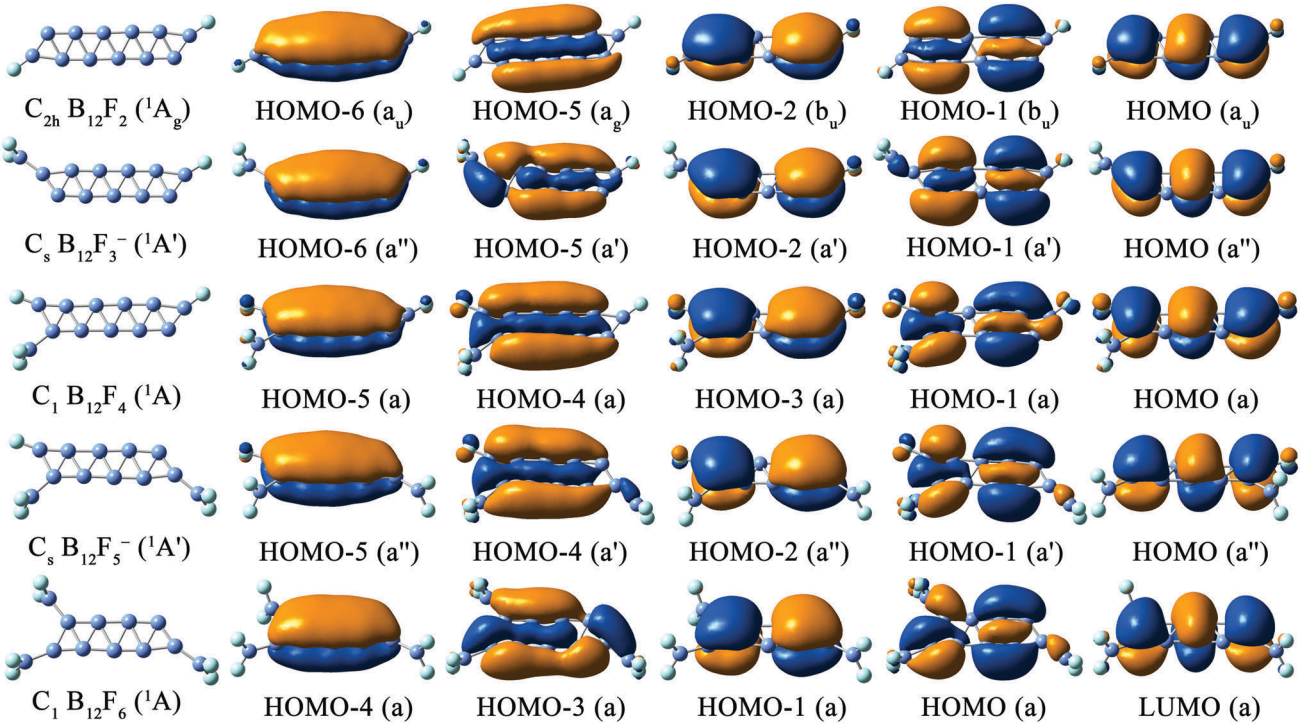

Fig. 4 Delocalized π and σ CMOs of the global-minima of $B_{12}F_n$ (n = 2, 4, 6) and $B_{12}F_n^-$ (n = 3, 5). The orbitals are aligned according to their shapes.

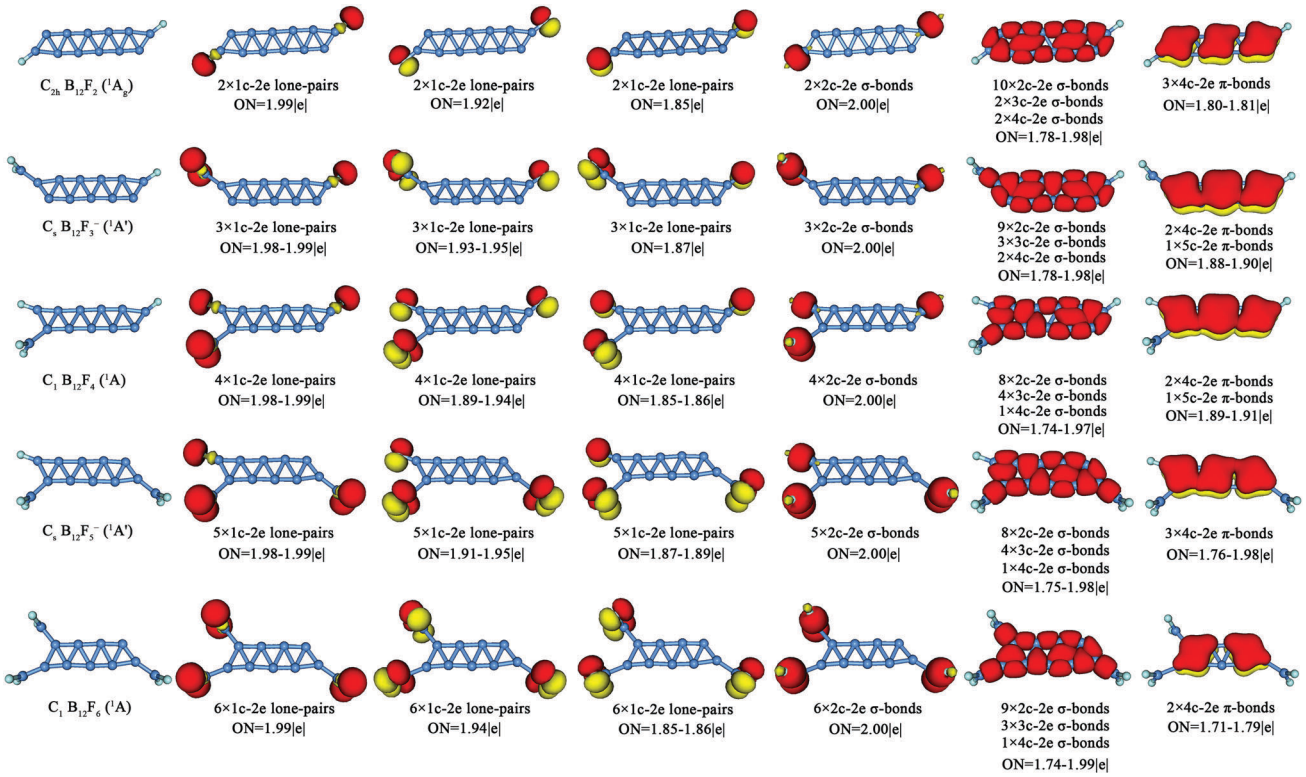

Fig. 5 The AdNDP bonding patterns of the global-minima of $B_{12}F_n$ (n = 2, 4, 6) and $B_{12}F_n^-$ (n = 3, 5).

aromatic system with two delocalized π CMOs (HOMO−1(a) and HOMO−4(a)) and two delocalized σ CMOs (HOMO(a) and HOMO−3(a)) which satisfies the Hückel 4n rule.

Detailed AdNDP analyses also unravel their bonding patterns in Fig. 5. Similar to $B_{12}H_2$,[35] C_{2h} $B_{12}F_2$ (**2**, ^1A_g) possesses two 2c-2e B–F σ-bonds (ON = 2.00 |e|), twelve 2c-2e and 3c-2e σ-bonds (ON = 1.78–1.98 |e|) along the peripheral B–B bonds, two 4c-2e σ-bonds with ON = 1.80 |e| and three 4c-2e π-bonds with ON = 1.80–1.81 |e| which form the unique σ plus π double conjugation and play critical roles in its stability. Owing to the existence of two F atoms, $B_{12}F_2$ (**2**, ^1A_g) also has six 1c-2e lone-pairs (ON = 1.85–1.99 |e|) around the F atoms. With the adding of F atoms, both C_s $B_{12}F_3^-$ (**9**, $^1A'$) and C_1 $B_{12}F_4$ (**4**, ^1A) form one BF_2 group at the corner of the central B_{11} unit and have similar bonding patterns. The BF_2 group is a common structural unit with high stability, which has been observed repeatedly in the crystallographic experiment of polyboron fluorides.[15,16,18] C_s $B_{12}F_3^-$ (**9**, $^1A'$) possesses nine 1c-2e lone-pairs with ON = 1.87–1.99 |e|, three 2c-2e B–F σ-bonds (ON = 2.00 |e|), twelve 2c-2e and 3c-2e σ-bonds (ON = 1.78–1.98 |e|), two 4c-2e σ-bonds (ON = 1.82–1.84 |e|), two 4c-2e π-bonds (ON = 1.82–1.84 |e|), and one 5c-2e π-bond (ON = 1.88–1.90 |e|). Compared with the bonding feature of C_s $B_{12}F_3^-$ (**9**, $^1A'$), C_1 $B_{12}F_4$ (**4**, ^1A) merely increases relevant three 1c-2e lone-pairs and one 2c-2e B–F σ-bond, but reduces one 2c-2e B–B σ-bond due to the distance of B–B connecting one B–F bond and the BF_2 group elongates to 1.73 Å in $B_{12}F_4$ (**4**) from 1.53 Å in $B_{12}F_3^-$ (**9**). C_s $B_{12}F_5^-$ (**11**, $^1A'$) also forms a typical BDC nanoribbon with two BF_2 groups and one F atom at the corner of the BDC B_{10} unit. Alternatively, it can be viewed as forming one B–F bond which is the key component of the new BF_2 group and breaking one peripheral B–B bond based on the configuration of $B_{12}F_4$ (**4**). Hence, owing to the increasing of the F atom, $B_{12}F_5^-$ (**11′**) only adds three 1c-2e lone-pairs and one 2c-2e B–F σ-bond in comparison with $B_{12}F_4$ (**4**). It is obvious that all of $B_{12}F_2$ (**2**), $B_{12}F_3^-$ (**9**), $B_{12}F_4$ (**4**) and $B_{12}F_5^-$ (**11**) are ribbon aromatic systems, where regular σ *versus* π alternation of the delocalized electron clouds along the BDC nanoribbons contributes to their stability from the AdNDP analyses in Fig. 5. The electron clouds distribute almost evenly on each part of the BDC nanoribbons, which maintain the optimal delocalized π or σ bonding within the $B_3/B_4/B_5$ units and effectively reduce the intramolecular electrostatic repulsion in the BDC systems. For C_1 $B_{12}F_6$ (**6**, ^1A), it has eighteen 1c-2e lone-pairs with ON = 1.85–1.99 |e| on the six F atoms, six 2c-2e B–F σ-bonds (ON = 2.00 |e|) and eleven 2c-2e and 3c-2e σ-bonds (ON = 1.74–1.96 |e|) around the peripheral B–B framework. The remaining one 3c-2e σ-bond with ON = 1.85 |e|, one 4c-2e σ-bond with ON = 1.85 |e| and two 4c-2e π-bonds (ON = 1.71–1.79 |e|) form the σ plus π double conjugation along the BDC B_9 unit but do not conform the electron counting rule of ribbon aromaticity.

Therefore, there are two reasons for the stability of the global minima of $B_{12}F_n^{0/-}$ (n = 1–6). On one hand, the ribbon aromaticity of the BDC nanoribbon $B_{12}F_n^{0/-}$ (n = 1–6) play a prominent role by means of reducing the intramolecular electrostatic repulsion to some extent. On the other hand, a mass of peripheral 2c-2e B–B σ-bonds exists in the BDC nanoribbons, which is an extremely vital stabilizing factor for planar boron clusters.

3.4 Simulated photoelectron spectroscopy of the global minima of $B_{12}F_n^-$ (n = 1–6)

To aid the future experimental characterization of $B_{12}F_n^-$ (n = 1–6) global minima, we also calculated herein the adiabatic and vertical detachment energies (ADE and VDE) of the ground-state $B_{12}F_n^-$ monoanions (n = 1–6) at TDDFT and simulated their photoelectron spectra. The simulated PES spectra are depicted in Fig. 6 and Fig. S13 (ESI†), where the spectra are constructed by fitting the distributions of 0.1 eV half-width and the electronic binding energies of the species well fall within the energy range of conventional excitation lasers (0–7 eV) in PES measurements.

The ADEs and VDEs of 2D quasi-planar C_s $B_{12}F^-$ (**7**, $^1A'$) and its iso-energetic isomer C_1 $B_{12}F^-$ (**7.1**, ^1A) that is similar to the global minima of $B_{12}X^-$ (X = H/Au/BO)[34] are predicted to be ADE = 3.92, 3.50 eV and VDE = 4.11, 3.68 eV, respectively, where the ADEs also represent the electron affinity (EAs) of C_s $B_{12}F$ (**1.3**, $^2A'$) and C_1 $B_{12}F$ (**1.1**, ^2A). It is more difficult to detach one

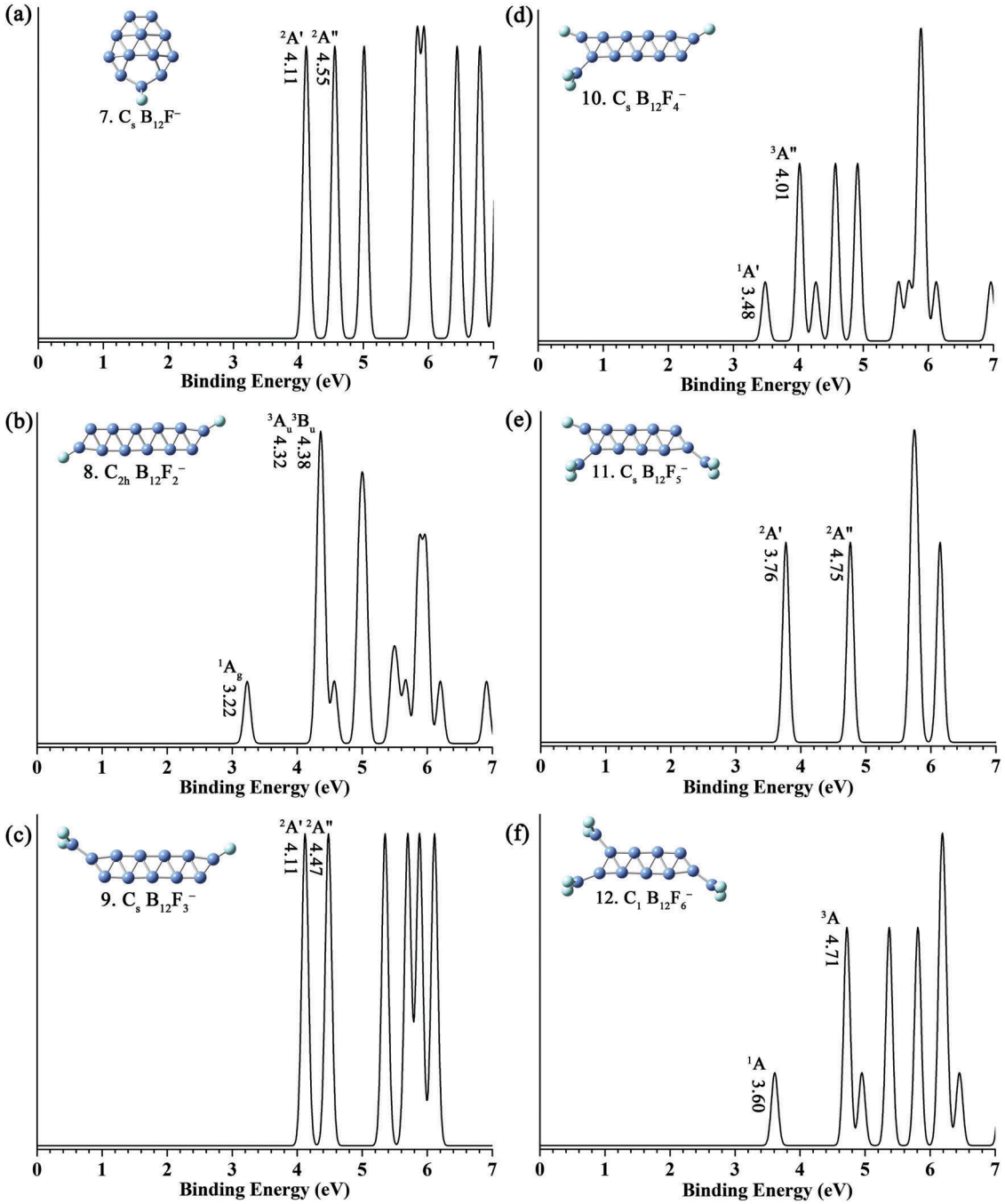

Fig. 6 Simulated photoelectron spectra based on the global minimum structures of $B_{12}F_n^-$ (n = 1–6) series. The simulations were done by fitting the distribution of the calculated VDEs with unit-area Gaussian functions of 0.1 eV halfwidth.

electron from C_s $B_{12}F^-$ (**7**, $^1A'$), thus C_s $B_{12}F^-$ (**7**, $^1A'$) is electronically robust. In Fig. S13 (ESI†), the X–A gaps between the ground-state band (X) and the first excited-state band (A) of C_s $B_{12}F^-$ (**7**, $^1A'$) and C_s $B_{12}F^-$ (**7.1**, $^1A'$) are 0.44 and 0.91 eV, respectively. Thus, the simulated photoelectron spectrum suggests that the 2D quasi-planar C_1 $B_{12}F$ (**1.1**, ^2A) is a more stable electronic structure and inert in chemistry. Similarly, the calculated ground state ADEs and VDEs for BDC $B_{12}F_n^-$ (n = 2–6) series at the B3LYP/6-311++G(d,p) level are ADE = 3.06, 3.97, 3.28, 3.57, 3.40 eV and VDE = 3.22, 4.11, 3.48, 3.76, 3.60 eV, respectively. The ADEs of BDC $B_{12}F_n^-$ (n = 2–6) corresponding to the EAs of their corresponding neutral species can be utilized to facilitate their future spectroscopic investigations. As shown in Fig. 6, the X–A gap of C_{2h} $B_{12}F_2^-$ (**8**, ^2A_g) is 1.10 eV, extremely close to the gaps (0.91, 0.99, and 1.11 eV) of C_1 $B_{12}F^-$ (**7.1**, ^1A), C_s $B_{12}F_5^-$ (**11**, $^1A'$), and C_1 $B_{12}F_6^-$ (**12**, ^2A). However, the simulated PESs of C_s $B_{12}F_3^-$ (**9**, $^1A'$) and C_s $B_{12}F_4^-$ (**10**, $^2A'$) are also depicted in Fig. 6(c) and (d), which exhibit a small energy gap (0.36 and 0.53 eV) between the first and second detachment transitions at the TDDFT level. We hope that the simulated spectra will facilitate future PES characterization of the global minima of $B_{12}F_n^-$ (n = 1–6) by taking full advantage of their VDEs and difference of X–A gaps.

3.5 F/H/Au/BO analogy

Nowdays, there is abundant theoretical and experimental evidence to confirm the H/Au/BO analogy.[34,37–40] In order to elucidate the validity of our theoretical prediction and explore the relationship between F and H/Au/BO, we compared the theoretical ADEs of $B_{12}X^-$ and $B_{12}X_2^-$ (X = F/H/Au/BO) systems at the B3LYP/6-311++G(d,p) level. It is worthwhile to state that similar to $B_{12}X_2^-$ (X = F/H/BO), the most stable $B_{12}Au_2^-$ also possesses a *trans* nanoribbon structure with two terminal Au bonding to the corners of the BDC B_{12} unit. As demonstrated in Fig. 7, the ADEs gradually increase from H to Au, F and BO in $B_{12}X^-$ [34] and $B_{12}X_2^-$ [37] (X = F/H/Au/BO) species. One significant reason is the effect of electronegativity of H, Au, F and the much more electron-withdrawing capacity of the BO σ radical. Moreover, it is notable that the ADEs of $B_{12}(BO)^-$ [34] and $B_{12}(BO)_2^-$ [37] are relatively large. First, the polar nature of the BO σ radical can induce substantial electrostatic stabilization to the $B_{12}(BO)_n^-$ (n = 1, 2) system, leading to the great ADEs for the monoanion clusters. Second, the partial participation of the BO σ radical in π conjugation leads to extend delocalization over the quasi-planar BDC B_{12} framework, which helps stabilize the π MOs and this sort of system as a whole.

In addition, we compared the simulated PES of C_1 $B_{12}F^-$ (**7.1**, ^1A) and C_{2h} $B_{12}F_2^-$ (**8**, ^2A_g) with the available PES in experiment of $B_{12}X^-$ (X = Au/BO)[34] and $B_{12}(BO)_2^-$ [37] as well. Amazingly, the ADE (3.50 eV) and VDE (3.68 eV) calculated for C_1 $B_{12}F^-$ (**7.1**, ^1A) at B3LYP correspond well to the ADE (3.48 eV) and VDE (3.59 eV) observed for $B_{12}Au^-$. Furthermore, the X–A gap (0.91 eV) of C_1 $B_{12}F^-$ (**7.1**, ^1A) also agrees surprisingly well with the X–A gap (0.96 eV) of $B_{12}Au^-$. Although the observed PES spectra of C_1 $B_{12}BO^-$ have a large blue shift due to electrostatic interactions, it displays well peak-to-peak correspondence to the PES spectra of C_1 $B_{12}F^-$ (**7.1**, ^1A). The excellent agreement provides powerful evidence for the F/Au/BO analogy. For C_{2h} $B_{12}F_2^-$ (**8**, ^2A_g), its ADE = 3.06 eV and VDE = 3.22 eV at the B3LYP level are slightly higher than the observed ADE (2.87 eV) and VDE (2.87 eV) of C_{2h} $B_{12}D_2^-$ [35] in experiment. The experimental ADE/VDE values (3.67/3.72 eV) of $B_{12}(BO)_2^-$ are in good agreement with the theoretical data (ADE/VDE: 3.68/3.78 eV).[37] Similarly, compared with C_{2h} $B_{12}F_2^-$ (**8**, ^2A_g), $B_{12}(BO)_2^-$ also exhibits a relatively large blue shift in the observed PES spectra, but it still shows the analogy between F and H/BO. Actually, the global minima of $B_{12}X^-$ and $B_{12}X_2^-$ (X = F/H/Au/BO) are similar, respectively, so this spectral similarity can be reflected by their structural similarity.

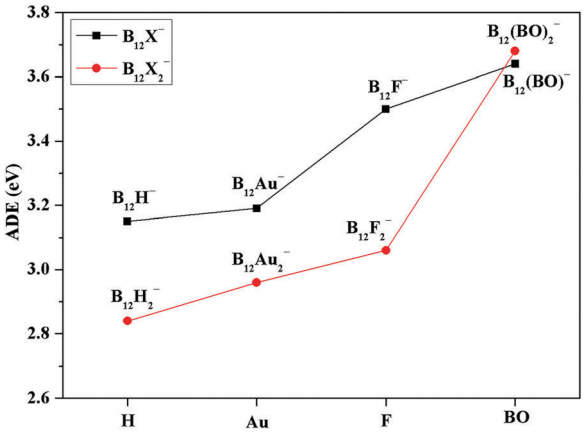

Fig. 7 Comparison of the theoretical ADEs of $B_{12}X^-$ and $B_{12}X_2^-$ (X = F/H/Au/BO) clusters at the B3LYP/6-311++G(d,p) level.

4. Conclusions

We have performed a systematic theoretical investigation into $B_{12}F_n^{0/-}$ (n = 1–6) species and found that it is unfeasible to reverse the relative stability of boron hydride $B_{12}H_n$ (n = 1–6) clusters by taking advantage of partial fluorination. Similar to previously reported perfectly planar D_{3h} $B_{12}H_6$ which is called as aromatic borozene, the planar fluorinated D_{3h} $B_{12}F_6$ (**6.7**, $^1A'$) also has a high-lying local minimum on the potential energy surface and almost can be ruled out from experiments under normal conditions. Our extensive and unbiased global minimum searches confirmed that with the exception of $B_{12}F^{0/-}$ nearly retaining the configuration of C_{3v} B_{12}, all the global minima of $B_{12}F_n^{0/-}$ (n = 2–6) species adopt BDC nanoribbon structures and start to form an extremely stable BF_2 group from n = 3. Comparing their representative 2D quasi-planar and 3D icosahedral isomers, a 2D-to-3D structural transformation occurs at n = 5 and n = 3 for $B_{12}F_n$ and $B_{12}F_n^-$ (n = 1–6) species, respectively. Bonding analyses reveal that the peripheral 2c-2e B–B σ-bonds and ribbon aromaticity play an indispensable role in stabilizing the $B_{12}F_n^{0/-}$ system. Our results also provide new cases for ribbon aromaticity that seems to be a general concept in nanoribbon systems. The simulated PES spectra of $B_{12}F_n^-$ (n = 1–6) may not only facilitate further experimental and

computational explorations, but also provide convincing evidence for the F/H/Au/BO analogy.

Conflicts of interest

The authors declare no competing financial interest.

Acknowledgements

This work was supported by the Key Projects of the National Natural Science Foundation of China (No. 21336006), the National Natural Science Foundation of China (No. 21776195 and 21573138), the National Natural Science Younger Foundation of China (No. 21703151), the Shanxi Province Science Foundation for Youths (No. 201601D202017), the Youth Foundation of Taiyuan University of Technology (No. 2015QN092 and No. 2016QN75), and the Scientific Research Fund for the Introduction of Talents from the Taiyuan University of Technology (No. tyut-rc201519a).

References

1 Q. Chen, W. J. Tian, L. Y. Feng, H. G. Lu, Y. W. Mu, H. J. Zhai, S. D. Li and L. S. Wang, *Nanoscale*, 2017, **9**, 4550–4557.
2 L. S. Wang, *Int. Rev. Phys. Chem.*, 2016, **35**, 69–142.
3 H. J. Zhai, Y. F. Zhao, W. L. Li, Q. Chen, H. Bai, H. S. Hu, Z. A. Piazza, W. J. Tian, H. G. Lu, Y. B. Wu, Y. W. Mu, G. F. Wei, Z. P. Liu, J. Li, S. D. Li and L. S. Wang, *Nat. Chem.*, 2014, **6**, 727–731.
4 E. Oger, N. R. M. Crawford, R. Kelting, P. Weis, M. M. Kappes and R. Ahlrichs, *Angew. Chem., Int. Ed.*, 2007, **46**, 8503–8506.
5 B. Kiran, S. Bulusu, H. J. Zhai, S. Yoo, X. C. Zeng and L. S. Wang, *Proc. Natl. Acad. Sci. U. S. A.*, 2005, **102**, 961–964.
6 H. J. Zhai, B. Kiran, J. Li and L. S. Wang, *Nat. Mater.*, 2003, **2**, 827–833.
7 (*a*) N. G. Szwacki, V. Weber and C. J. Tymczak, *Nanoscale Res. Lett.*, 2009, **4**, 1085–1089; (*b*) N. G. Szwacki and C. J. Tymczak, *Nanoscale Res. Lett.*, 2012, **7**, 236–241.
8 G. Forte, A. La Magna, I. Deretzis and R. Pucci, *Nanoscale Res. Lett.*, 2010, **5**, 158–163.
9 Y. Ohishi, K. Kimura, M. Yamaguchi, N. Uchida and T. Kanayama, *J. Phys.: Conf. Ser.*, 2009, **176**, 012030.
10 H. Bai and S. D. Li, *J. Cluster Sci.*, 2011, **22**, 525–535.
11 S. Sahu and A. Shukla, *Nanoscale Res. Lett.*, 2010, **5**, 714–719.
12 (*a*) Y. Ohishi, K. Kimura, M. Yamaguchi, N. Uchida and T. Kanayama, *J. Chem. Phys.*, 2008, **128**, 124304; (*b*) Y. Ohishi, K. Kimura, M. Yamaguchi, N. Uchida and T. Kanayama, *J. Chem. Phys.*, 2010, **133**, 074305.
13 A. R. Pitochelli and F. M. Hawthorne, *J. Am. Chem. Soc.*, 1960, **82**, 3228–3229.
14 N. G. Szwacki, *Nanoscale Res. Lett.*, 2008, **3**, 49–54.
15 J. A. J. Pardoe, N. C. Norman, P. L. Timms, S. Parsons, I. Mackie, C. R. Pulham and D. W. H. Rankin, *Angew. Chem., Int. Ed.*, 2003, **42**, 571–573.
16 P. L. Timms, N. C. Norman, J. A. J. Pardoe, I. D. Mackie, S. L. Hinchley, S. Parsons and D. W. H. Rankin, *Dalton Trans.*, 2005, 607–616.
17 H. Bai, Q. Chen, C. Q. Miao, Y. W. Mu, Y. B. Wu, H. G. Lu, H. J. Zhai and S. D. Li, *Phys. Chem. Chem. Phys.*, 2013, **15**, 18872–18880.
18 L. Trefonas and W. N. Lipsomb, *J. Chem. Phys.*, 1958, **28**, 54–55.
19 K. A. Solntsev, A. M. Mebel, N. A. Votinova, N. T. Kuznetsov and O. P. Charkin, *Koord. Khim.*, 1992, **18**, 340–364.
20 D. V. Peryshkov, A. A. Popov and S. H. Strauss, *J. Am. Chem. Soc.*, 2009, **131**, 18393–18403.
21 H. Thomsen, O. Haeckel, U. Krause and W. Preetz, *Z. Anorg. Allg. Chem.*, 1996, **622**, 2061–2064.
22 E. V. Bukovsky, K. W. Lui, D. V. Peryshkov and S. H. Strauss, *Abstr. Pap. Am. Chem. Soc.*, 2011, **242**, 1.
23 D. V. Peryshkov, E. V. Bukovsky, T. C. Folsom and S. H. Strauss, *Polyhedron*, 2013, **58**, 197–205.
24 D. Yu. Zubarev and A. I. Boldyrev, *Phys. Chem. Chem. Phys.*, 2008, **10**, 5207–5217.
25 D. J. Wales and J. P. K. Doye, *J. Phys. Chem. A*, 1997, **101**, 5111–5116.
26 A. D. Becke, *J. Chem. Phys.*, 1993, **98**, 5648–5652.
27 C. Lee, W. Yang and R. G. Parr, *Phys. Rev. B: Condens. Matter Mater. Phys.*, 1988, **37**, 785–789.
28 (*a*) J. S. Binkley, J. A. Pople and W. J. Hehre, *J. Am. Chem. Soc.*, 1980, **102**, 939–947; (*b*) M. S. Gordon, J. S. Binkley, J. A. Pople, W. J. Pietro and W. J. Hehre, *J. Am. Chem. Soc.*, 1982, **104**, 2797–2803; (*c*) W. J. Pietro, M. M. Francl, W. J. Hehre, D. J. Defrees, J. A. Pople and J. S. Binkley, *J. Am. Chem. Soc.*, 1982, **104**, 5039–5048; (*d*) T. Clark, J. Chandrasekhar, G. W. Spitznagel and P. V. R. Schleyer, *J. Comput. Chem.*, 1983, **4**, 294–301.
29 M. J. Frisch, G. W. Trucks, H. B. Schlegel and G. E. Scuseria, *et al.*, *Gaussian 09, Revision B.01*, Gaussian, Inc., Walligford CT, 2010.
30 (*a*) J. Cizek, *Adv. Chem. Phys.*, 1969, **14**, 35–89; (*b*) G. E. Scuseria and H. F. Schaefer, *J. Chem. Phys.*, 1989, **90**, 3700–3703; (*c*) R. J. Bartlett and M. Musial, *Rev. Mod. Phys.*, 2007, **79**, 291–352; (*d*) J. P. Perdew, K. Burke and M. Ernzerhof, *Phys. Rev. Lett.*, 1996, **77**, 3865–3868; (*e*) J. P. Perdew, K. Burke and M. Ernzerhof, *Phys. Rev. Lett.*, 1997, **78**, 1396; (*f*) C. Adamo and V. Barone, *J. Chem. Phys.*, 1999, **110**, 6158–6170.
31 T. Lu and F. W. Chen, *J. Comput. Chem.*, 2012, **33**, 580–592.
32 U. Varetto, *MOLEKEL, version 5.4*, Swiss National Supercomputing Centre, Lugano, Switzerland, 2009.
33 (*a*) M. E. Casida, C. Jamorski, K. C. Casida and D. R. Salahub, *J. Chem. Phys.*, 1998, **108**, 4439–4449; (*b*) R. Bauernschmitt and R. Ahlrichs, *Chem. Phys. Lett.*, 1996, **256**, 454–464.
34 H. Bai, H. J. Zhai, S. D. Li and L. S. Wang, *Phys. Chem. Chem. Phys.*, 2013, **15**, 9646–9653.
35 W. L. Li, C. Romanescu, Z. A. Piazza and L. S. Wang, *J. Am. Chem. Soc.*, 2012, **134**, 13228–13231.

36 D. Z. Li, Q. Chen, Y. B. Wu, H. G. Lu and S. D. Li, *Phys. Chem. Chem. Phys.*, 2012, **14**, 14769–14774.
37 H. J. Zhai, Q. Chen, H. Bai, H. G. Lu, W. L. Li, S. D. Li and L. S. Wang, *J. Chem. Phys.*, 2013, **139**, 174301.
38 A. N. Alexandrova, E. Koyle and A. I. Blodyrev, *J. Mol. Model.*, 2006, **12**, 569–576.
39 (*a*) D. Y. Zubarev, A. I. Boldyrev, J. Li, H. J. Zhai and L. S. Wang, *J. Phys. Chem. A*, 2007, **111**, 1648–1658; (*b*) W. Z. Yao, J. C. Guo, H. G. Lu and S. D. Li, *J. Phys. Chem. A*, 2009, **113**, 2561–2564; (*c*) H. J. Zhai, C. Q. Miao, S. D. Li and L. S. Wang, *J. Phys. Chem. A*, 2010, **114**, 12155–12161; (*d*) H. J. Zhai, J. C. Guo, S. D. Li and L. S. Wang, *ChemPhysChem*, 2011, **12**, 2549–2553; (*e*) Q. Chen, H. J. Zhai, S. D. Li and L. S. Wang, *J. Chem. Phys.*, 2012, **137**, 044307.
40 D. Yu. Zubarev, J. Li, L. S. Wang and A. I. Boldyrev, *Inorg. Chem.*, 2006, **45**, 5269–5271.